PCCP

Accepted Manuscript

ROYAL SOCIETY OF CHEMISTRY

www.rsc.org/pccp

Cite this: DOI: 10.1039/c0xx00000x

www.rsc.org/xxxxxx

ARTICLE TYPE

Fractal-like electrode based on double-wall nanotube of anatase and exhibiting improved electrochemical behaviour in both lithium and sodium batteries

José R. González,[a] Ekaterina Zhecheva,[b] Radostina Stoyanova,[b] Diana Nihtianova[c,b], Pavel Markov,[b] Régis Ravelle Chapuis,[d] Ricardo Alcántara,[a*] Francisco Nacimiento,[a] José L. Tirado[a] and Gregorio F. Ortiz[a]

Received (in XXX, XXX) Xth XXXXXXXXX 20XX, Accepted Xth XXXXXXXXX 20XX
DOI: 10.1039/b000000x

An anatase nanotube array has been prepared with a special morphology: two concentric walls and a very small central cavity. The method used here to achieve the double-wall structure is a single-step anodization under a voltage ramp. Thanks to this nanostructure, which is equivalent to a fractal electrode, the electrochemical behaviour is improved, and the specific capacity is higher in both lithium and sodium cells due to pseudocapacitance. The double-wall structure of the nanotube enhances the surface of TiO_2 being in contact with the electrolyte solution, thus allowing an easy penetration of the alkali ions into the electrode active material. The occurrence of sodium titanate in the electrode material after electrochemical reaction with sodium is studied by using EPR, HRTEM and NMR.

1. Introduction

Titanium dioxide has been described by several authors as one of the most promising materials for new applications related with energy storage and conversion, due to its interesting properties, very low toxicity and economic price. Regarding materials for Li-ion batteries, this material has attracted the attention of a great number of scientists.[1-6] Thus, TiO_2 in the anatase form is an important candidate to replace graphite, not only owing to high theoretical gravimetric and volumetric capacities vs. lithium (335.4 mAh g^{-1} and 1308.1 mAh cm^{-3} for $LiTiO_2$) but also due to its higher and more stable lithiation and delithiation voltage that can provide safer batteries. However, the practical capacity values are usually below the maximum theoretical capacities, and the amount of lithium that is inserted into anatase is affected by particle size, lithium diffusion distances, lattice defects and other factors.[6,7] The possibility of controlling the dimensions and crystallinity of the nanoparticles could be exploited to fabricate a more geometrically appropriate electrodes, designed to improve the electrochemical performance in batteries. Within the known nano-architectures of TiO_2, one of the most interesting morphologies is built by self-organized nanotube (nt-TiO_2). The vertically aligned nanotube arrays allow rapid lithium diffusion and has been proposed as electrode material for microbatteries.[8,9] nt-TiO_2 can be easily prepared by electrochemical oxidation of a titanium foil in fluoride-ion containing electrolytes.[10,11] For a fixed anodization voltage and electrolyte composition, the increase in nanotube length with time follows the parabolic law and, on the other hand, the nanotube diameter depends mainly on the anodization voltage.[10,11] Although the material obtained by titanium anodization is XRD-amorphous, it is suitable for being thermally treated to obtain a crystalline phases (e.g. anatase or rutile) while the primary nanotube structure is preserved.

The areal capacity (mAh cm^{-2} units) of the electrode can be increased by using longer nanotubes. However, the full gravimetric capacity (mAh g^{-1} units) is not reached for the longer nt-TiO_2 due to the longer lithium diffusion path.[11] Wei et al. recently reported highly ordered TiO_2 nanotube arrays with high aspect ratio (about 60) and with areal capacities of 0.24 mAh cm^{-2} (i.e. 96 mAh g^{-1}) vs. lithium at 2.5 mA cm^{-2} current density, and 0.46 mA h cm^{-2} at 0.05 mA cm^{-2}.[1] The same authors also found that, for two-step anodized nt-TiO_2, the walls of the anatase nanotubes contain two types of crystalline layers: the inner wall layer (32 nm) and the outer wall layer (15 nm thick). In addition, they revealed that nt-TiO_2 with thinner walls gave lower areal capacities.

Besides lithium, anatase can also react reversibly with sodium.[11-13] Although it was believed that the capacity of anatase in sodium cells was smaller than in lithium cells, two independent research groups have very recently reported that the nanostructure of the anatase particles can be modified to achieve improved capacity values.[12,13]

In this study, we obtain a self-organized array of anatase nanotubes, in which the nanotubes have double walls, by smart tuning of the anodization parameters. These concentric nanotubes have improved geometrical dimensions to provide higher contact surface between electrolyte solution and electrode, shorter diffusion distances, better mechanical stability and as a product of all that, better electrochemical behaviour in both lithium sodium

batteries. To better understand of the reaction mechanisms and to characterize the obtained materials SEM, TEM, XRD, EPR, and NMR experiments have been carried out.

2. Experimental

2.1 Preparation of TiO_2 nanotubes

The anodization process of titanium metal foil was used to prepare self-organized titania nanotube arrays. The counter electrode was a Pt foil, and the electrolyte solution was an ethylene glycol/water (98:2) mixture containing 0.3 wt % of NH_4F as the electrolyte salt. The anodization process of titanium under fixed voltage was performed by applying 100 V during 2 h. The anodization of titanium under a voltage ramp was carried out by continuously increasing the anodization voltage from 20 to 100 V during 2 h (11.1 mV s^{-1} ramp). The obtained nanotubes were extensively rinsed to remove fluoride ions. To prepare anatase nanotubes, nt-TiO_2 samples were annealed at 550°C in air atmosphere during 3 h. The imposed annealing temperature was selected as the highest possible temperature to obtain rutile-free anatase.

2.2 Characterization of materials

XRD patterns were recorded in a Siemens D5000 instrument with CuKα radiation.

The SEM micrographs were obtained using secondary electrons detector in a JSM6300 instrument or, alternatively, with a JSM7800F. The TEM investigations were performed on a JEOL 2100 instrument and a JEOL 2100 XEDS: Oxford Instruments, X-MAX^N 80T CCD Camera ORIUS 1000, 11 Mp, GATAN at accelerating voltage of 200 kV. The specimens were prepared by grinding and dispersing them in ethanol by ultrasonic treatment for 6 minutes. The suspensions were dripped on standard holey carbon/copper grids. The measurements of lattice-fringe spacing recorded in HRTEM micrographs were made using digital image analysis of reciprocal space parameters. The analysis was carried out by the Digital Micrograph software.

The EPR spectra were recorded as the first derivative of the absorption signal of an ERS-220/Q spectrometer within the temperature range of 90-400 K. The g factors were determined with respect to a Mn^{2+}/ZnS standard. The signal intensity was established by double integration of the experimental EPR spectrum.

^{23}Na MAS NMR spectra were recorded using a Bruker Avance 400 WB instrument, at 13 kHz of spin rate. The reference (δ=0 ppm) was NaCl aqueous solution.

2.3 Electrochemical tests

The electrochemical behaviour of nt-TiO_2 electrode material was studied in a VMP-type apparatus (Biologic Science Instruments). For this purpose, the electrochemical test cells (Swagelok-type) were mounted in a dry-box filled with Ar. The positive electrode was nt-TiO_2 supported in the Ti-substrate, and previously rinsed with water and dried under vacuum at 120°C overnight. No binder was used in the electrodes.

In the case of lithium test cells, a piece of Li was used as negative electrode, and the electrolyte solution was 1 M $LiPF_6$ in ethylene carbonate:diethyl carbonate (EC:DEC=1:1) solvents mixture

For sodium cell, a piece of Na was used like negative electrode. The electrolyte solution was 1 M $NaPF_6$ in ED:DEC=1:1 solvents mixture and containing a 5% of fuoroethylene carbonate (FEC) as additive.

3. Results and discussion

3.1 Transient curves

The formation of nt-TiO_2 can be followed by recording the transient curves of titanium anodization (Fig. 1).[2,11]. The anodization under fixed voltage starts with a strong decrease of the current density which corresponds to formation of the compact layer of TiO_2 on the Ti substrate in the presence of oxygen. Then, the observed increase in current density is due to dissolution of TiO_2 in the presence of fluoride ions and formation of pores. Finally, the nearly constant current density (ca. 240 A m^{-2} after ca. 80 min) is ascribed to the growth of titania nanotubes under steady state conditions, between oxide formation and titanium dissolution in the form of fluoro-complexes.

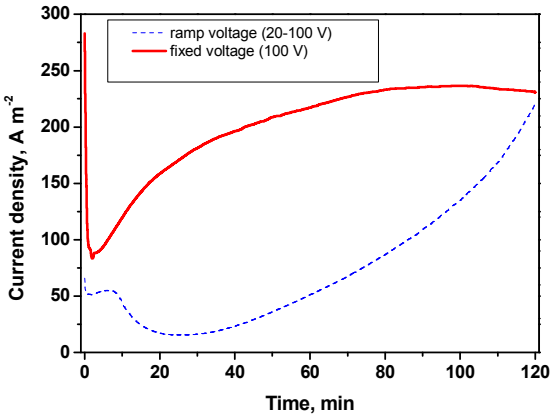

Fig. 1 Transient curves obtained for anodization of titanium under fixed voltage (100 V, 120 min) or under ramp voltage (from 20 V to 100 V, during 20 min).

The transient curve is modified by applying a voltage ramp (Fig. 1), and this fact can influence on the mechanism of nanotube formation. A minimum of current density (ca. 15 A m^{-2}) is observed after ca. 25 min of anodization time, then the current density increases exponentially with time and, on the contrary to fixed voltage, the steady state is not observed. The migration of the ions through the anodized titanium film can be affected by the voltage ramp and the modification of the electric field strength. Since the migration rates are different for fluoride, oxide and titanium ions, the continuous change of the applied electric field may induce a gradient of composition in the film, generating stress in the nanotube structure and finally the breakdown of the nanotube wall into two concentric nanotubes. The conversion of Ti to TiO_2 involves expansion in volume and, although the stress can induce plastic flow of the oxide and tube formation, it seems that under the continuous change of the electric field and ion migration rates the single-walled nanotube wall can break into double-walled nanotube. The rapid migration rate of the fluoride ions trough the stressed regions of nt-TiO_2 also may induce

etching and separation of the nanotube wall. On the other hand, the resulting lower current density leads to a slower rate of nanotube growth.

3.2 Nanotube structure and morphology

After anodization of titanium and prior to annealing, the obtained nt-TiO_2 are XRD-amorphous (see electronic supplementary information, Fig. S1). After heating nt-TiO_2 in air atmosphere to 550°C, the anatase phase is obtained.

The morphology of nt-TiO_2 samples was examined by using SEM and TEM (Fig. 2). The nanotubes grow perpendicularly to the Ti-substrate which is equivalent to an epitaxial growth.[13] The nanotubes self-array obtained by anodization under fixed voltage (100 V, 2 h) forms a film of thickness (nanotube length) of ca. 67 µm (Fig. 2A-C). The inner diameter of the nanotube (cavity which runs parallel to the nanotube axis) is ca. 90 nm, and the nanotube wall thickness is ca. 30 nm. (Fig. 2B). The corresponding anatase sample exhibiting this nanotube morphology with a single wall can be named as SWANT (single-wall anatase nanotube).

After anodization using a ramp of voltage from 20 to 100 V during 2 h, self-organized titania nanotubes are formed with an average nanotube length of about 6 µm (Fig. 2D-G). The outer nanotube (or total) diameter is ca. 200 nm (Fig. 2E). The diameter of the inner central cavity which runs parallel to the nanotube axis is ca. 40 nm. The nanotube exhibits two concentric walls (outer wall and inner wall). The outer wall is relatively thinner (about 20 nm), while the inner wall is thicker (about 45 nm). The inner wall of the external nanotube and the outer wall of the internal tube are slightly separated, and the distance between the two walls is ca. 10 nm. The anatase sample exhibiting nanotube morphology with two concentric walls can be named DWANT (double-wall anatase nanotube). The diameter of the inner nanotube cavity is smaller for the samples prepared under voltage ramp, and this fact can increase the apparent density of the electrode active material, while the contact surface between the nanotube surface and the electrolyte solution does not decrease due to the cylindrical cavity between the two concentric nanotubes. For a fixed nanotube length, the occurrence of a concentric two-nanotubes structure can increase the total surface area by a factor of 225 %. The special morphology of the double-wall nanotube lets us to consider it a fractal-like electrode maximizing surface-to-volume ratio.

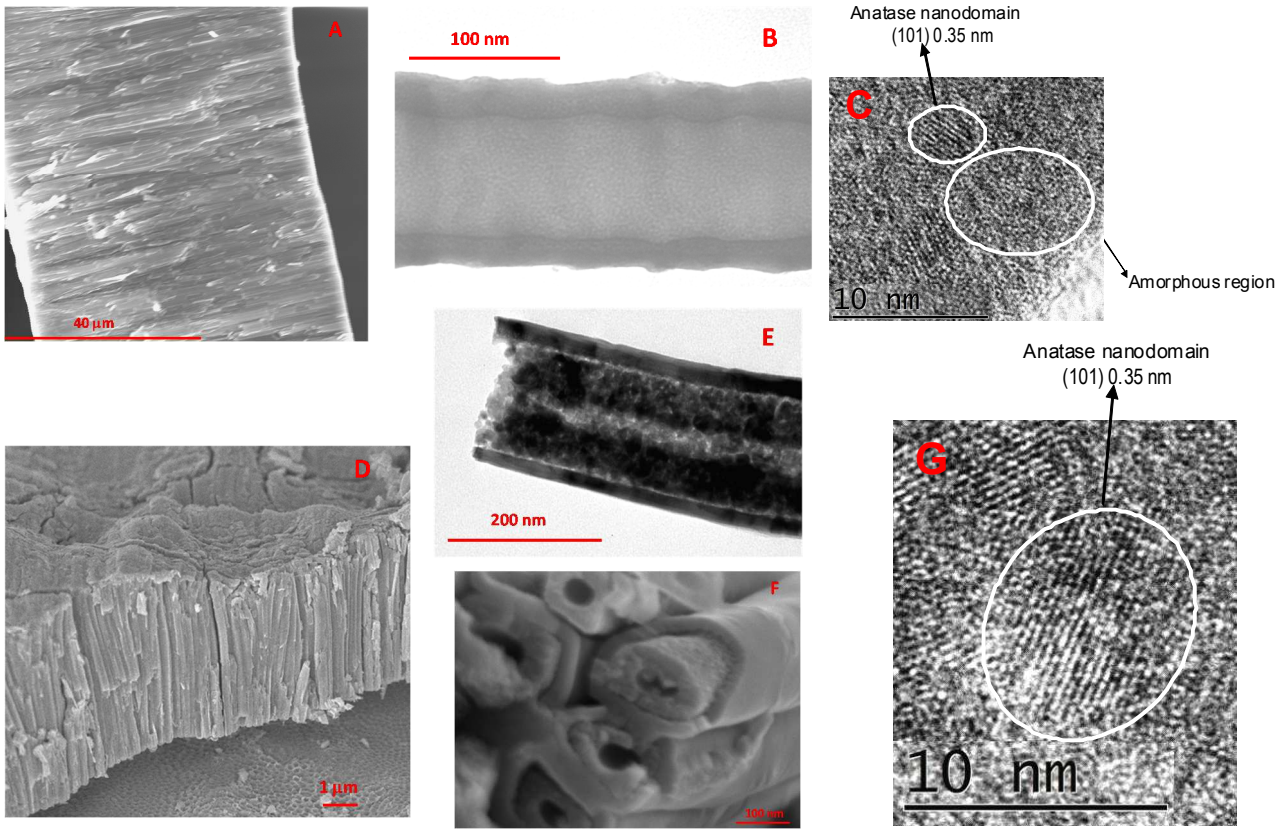

Fig.2 SEM and TEM micrographs for nt-TiO_2: (A-C) single-wall (fixed voltage anodization) and (D-G) double-wall (ramp voltage anodization).

Although as-prepared titania nanotubes obtained by anodization of titanium are XRD-amorphous, HRTEM images of both single-wall (Fig. 2C) and double-wall (Fig. 2G) nt-TiO_2 reveal few and very small crystalline domains. The size of these crystalline nanodomains seems to be lower for single-wall nanotube (about 4 nm) than double-wall nanotube (10-14 nm). In addition, the nanocrystalline domains are ascribed to anatase phase and are more often found for double-wall nanotube. On the

other hand, fluoride atoms homogenously distributed in the nanotube were detected by EDS microanalysis, suggesting that $TiO_{2-x}F_{2x}$ is formed. The fluorine ions content is higher for SW-TiO_2 (11.5% at.) than DW-TiO_2 (8.4% at.), because the longer nanotubes trap more fluoride ions. After annealing at 550 °C, the observed crystalline nanodomains grow up to ca. 30 nm for SWANT and DWANT. The grain growth process is concomitant with a loss of fluorine and crystallization of the pure anatase phase.

3.3 Electron Paramagnetic Resonance

The analysis of the defect structure of titania nanotube was carried out by EPR and the transformation of the amorphous into crystalline nanotubes was monitored. This technique has been demonstrated to be informative in respect of differentiating the trapped charges in the surface and the bulk of TiO_2 having anatase or rutile type structure.[14,15] This is a simple consequence of the different spin states for titanium ions: while Ti^{4+} is a diamagnetic ion, Ti^{3+} with the ^2D configuration yields a characteristic EPR spectrum. The EPR spectra of as-prepared and annealed nt-TiO_2 samples are collected on Fig. 3. The EPR spectra of the as-prepared SW-TiO_2 and DW-TiO_2 consist of two overlapping signals: a narrow asymmetric signal with a g-tensor of $g_\perp$=1.99, an unresolved $g_\parallel$ and a line width of about 0.2 mT; a broad nearly symmetric signal with g=1.94 and a line width of 12 mT. The broad signal has a stronger intensity as compared with the narrow signal (Table 1).

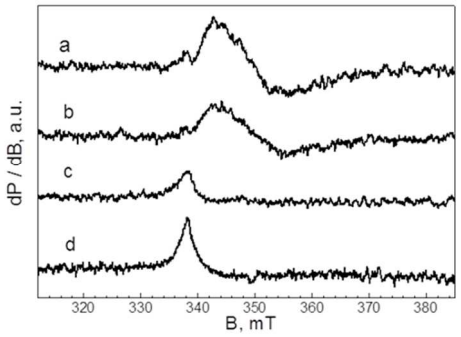

Fig. 3 EPR spectra recorded at 78 K for nt-TiO_2 samples: (a) amorphous double-wall, (b) amorphous single-wall, (c) anatase double-wall and (d) anatase single-wall.

Table 1 Relative EPR intensities of narrow and broad signals due to the lattice and surface anatase electron trapping sites ($I_{lattice}$ and $I_{surface}$, respectively).

nt-TiO_2 sample	$I_{lattice}$, a.u.	$I_{surface}$, a.u.	$I_{surface}/I_{lattice}$
Amorphous, double-wall	1.0	3.1	3.1
Amorphous, single-wall	0.8	3.2	4.2
Anatase, double-wall	3.7	0	0
Anatase, single-wall	5.8	0	0

After annealing the nt-TiO_2 at 550° C, the broad signal disappears, whereas the narrow signal grows in intensity. Both EPR signals display g-values that fall in the range which is typical for Ti^{3+} ions. The g-tensor for the narrow signal coincides with that for Ti^{3+} in regular lattice sites of the anatase matrix ($g_\perp$=1.990 and $g_\parallel$=1.957), while the g-values of the broad signal allow its attribution to surface anatase electron trapping sites.[16] The different line widths of the signals are a further proof for their assignment. Every Ti^{3+} ion occupying a regular crystal site has a fixed local coordination, which gives rise to a relatively lower EPR line width. On the contrary, Ti^{3+} ions on the nanotube surface are characterized by a structural inhomogeneity regarding local coordination, crystal field symmetry, and the presence of ligands such as $OH^-/O^{2-}/F^-$, which are a driving force for the broadening of the EPR signal. This suggestion is further supported by data from EDS microanalysis on the fluorine content in nt-TiO_2. Therefore, we are able to assign the broad signal to Ti^{3+} ions having mainly F^- ions as ligands. After annealing at 550°C, the release of F^- ions is concomitant with a disappearance of the broad signal. However, even at 550 °C, the bulk defects remain.

3.4 Electrochemical cycling in lithium cell

In Fig. 4A,B, the electrochemical behaviour of DWANT under galvanostatic conditions is compared in lithium cell with that of SWANT. The capacity values have been normalized by the finger print area of the electrode and the average nanotube length (measured by sample examination with SEM). The maximum theoretical capacity for a dense film of anatase would be 131 μAh cm^{-2} μm^{-1} (corresponding to $LiTiO_2$). The values for SWANT are well below the maximum theoretical capacity (Fig. 4A). Higher values of capacity are obtained for DWANT (Fig. 4B), being in the range between ca. 170 and 70 μAh cm^{-2} μm^{-1}, depending on the imposed current density. These values are higher than other previously reported in the literature for anatase nt-TiO_2 in lithium cell.[2,5,17] Most probably, the increase in specific capacity is due to the short nanotube length, the double-wall structure and the larger surface of the fractal electrode material which is exposed to the electrolyte solution. In addition, the rigidity of the two-wall structure to accept bulk defects may also explain the higher capacity, according to the EPR results. Apparently, lithium insertion is easier in the lattice of DWANT which has less bulk defects. The double-wall structure allows buffering the volume changes due to insertion/extraction of lithium into/from the anatase framework, which helps preserving the electrode integrity, and also enhances the surface of nt-TiO_2 in contact with the electrolyte solution allowing a rapid penetration of the lithium ions into the electrode. The small size of the central cavity leads to a higher density of active material per footprint area (for a given value of nanotube length), and consequently higher capacity. On the other hand, Shin et al reported that the concentration of defects affects the diffusivity of lithium in TiO_2.[18]

Typical potential-capacity curves are shown in Fig. 4C. The plateaus, which are due to structural transitions and coexistence of two phases, are observed in good agreement with the literature.[7] The structure transition was further studied by using XRD and these results can be found in the supplementary

information.

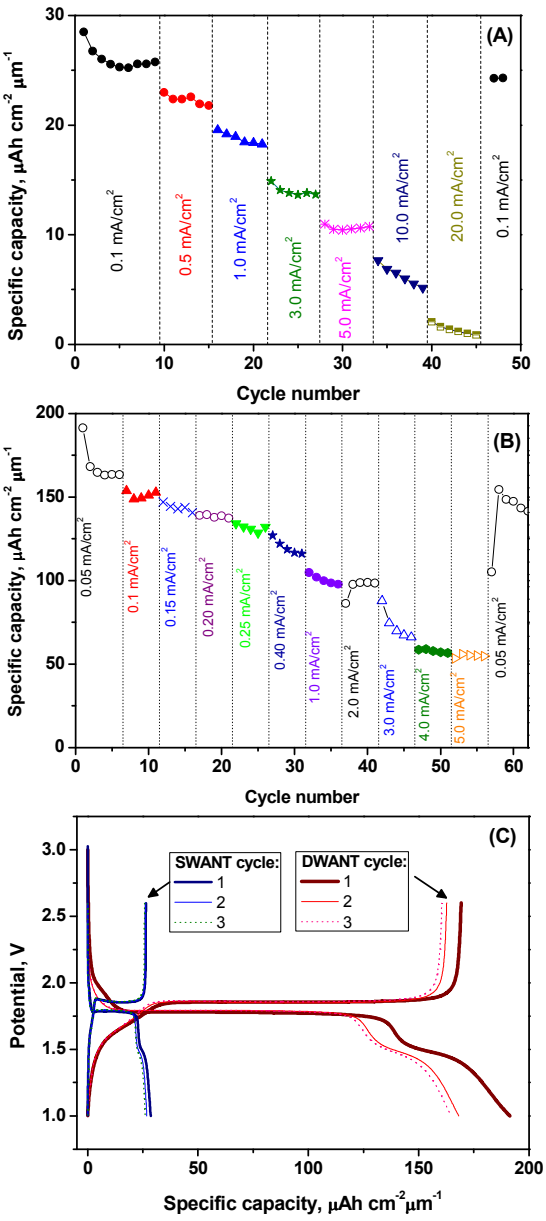

Fig. 4 Specific capacities as a function of cycle number for galvanostatic cycling lithium test cell of SWANT (with average length L= 67 μm) (A) and DWANT (L=6 μm) (B). The lithium cells were cycled in the range between 1.0 and 2.6 V under variable current density. (C) Potential-capacity curves corresponding to the first three cycles which are shown in (A) and (B).

On the other hand, we have also prepared SWANT with a shorter length (about 12 μm of length) using fixed voltage anodization (100 V during 15 min). By comparing the resulting electrochemical behaviour under variable current density of short-length SWANT (Fig. 5) and short-length DWANT (Fig. 4B), we can further confirm that the double-wall structure results in a net improvement of the specific capacity and better response to fast kinetics.

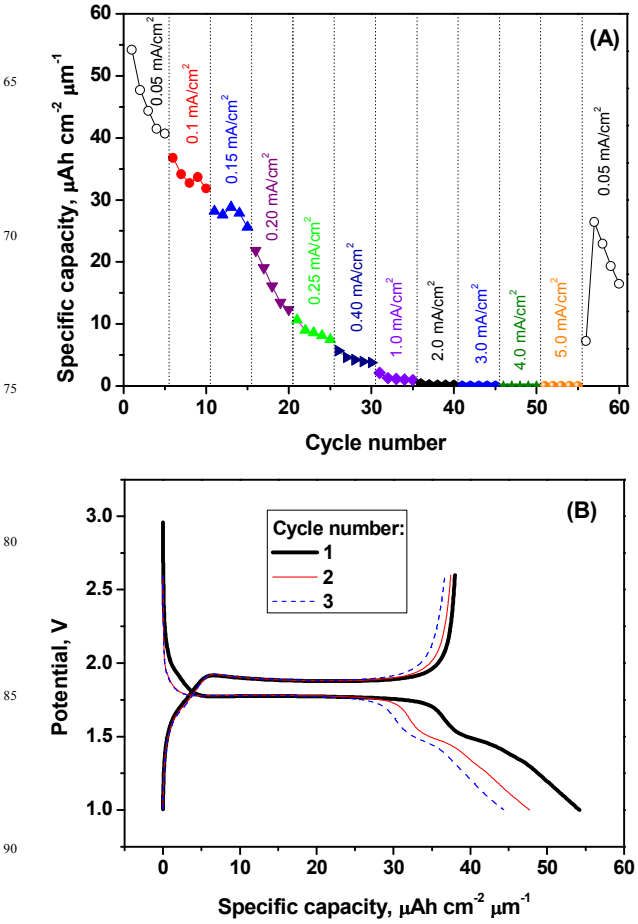

Fig.5 Galvanostatic cycling results in lithium test cell of SWANT (anodization under fixed voltage) with average length L=12 μm. (A) Specific capacities as a function of cycle number. (B) Corresponding potential-capacity curves of the first three cycles. The lithium cells were cycled in the range between 1.0 and 2.6 V under variable current density (from 0.05 mA m^{-2} to 5 mA cm^{-2}).

3.5 Electrochemical cycling in sodium cell

In sodium cell (Fig. 6A), the electrode active material obtained by ramp voltage, or DWANT, also shows higher specific capacity value in comparison with SWANT and irrespectively of the nanotube length. The reaction between sodium and anatase may be very strongly affected by the adsorption of sodium in the surface of nt-TiO_2 and, on the other hand, there is no plateau of biphasic transformation in the potential-capacity curves (Fig. 6B,C). Having in mind the absence of plateau, the imposed lower potential limit was 0.01 V. On the other hand, the composition of the electrolyte is a key parameter to achieve the electrochemical cycling of anatase in sodium cell.[12,13] Most probably, the special morphology of the nanotubes and the enhanced contact between the solid electrode and the liquid electrolyte solution allow the storage of a large amount of sodium the nanotube surface and a very large capacity is then achieved. The behaviour of the negative electrode (Na) and electrolyte decomposition can affect to the cycling of the cell, particularly for 0.01 V of lower cut-off potential. The double-wall nanotube exhibits better cycling

stability for a lower cut-off potential of 0.01 V.

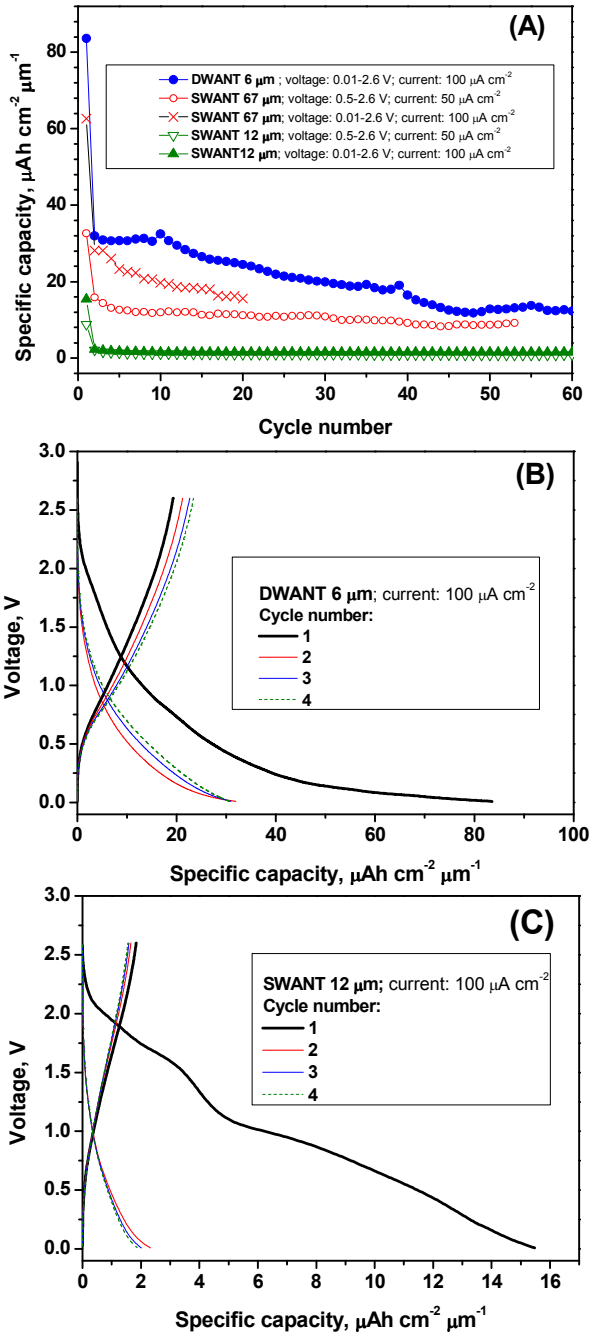

Fig. 6 Electrochemical results for SWANT and DWANT in sodium test cells under fixed current density (50 or 100 μA cm^{-2}). (A) Capacity as a function of cycle number. (B) Voltage-capacity curves for DWANT. (C) Voltage-capacity curves for SWANT.

3.6 Electrochemical mechanism in lithium cell

Two main mechanisms can contribute to the reversible electrochemical reaction between anatase and lithium: lithium insertion into the anatase lattice and accommodation of lithium in the surface of TiO_2 particles. Although the electrochemical insertion of lithium into anatase has been studied in the literature, besides measuring the overall capacity, it is also important to understand the mechanism of lithium accommodation in order to find any possible differences between SWANT and DWANT. The method used here is the determination of the b-parameter in the relationship between current density (i) and scan rate (v): $i=av^b$.[13,19,20]

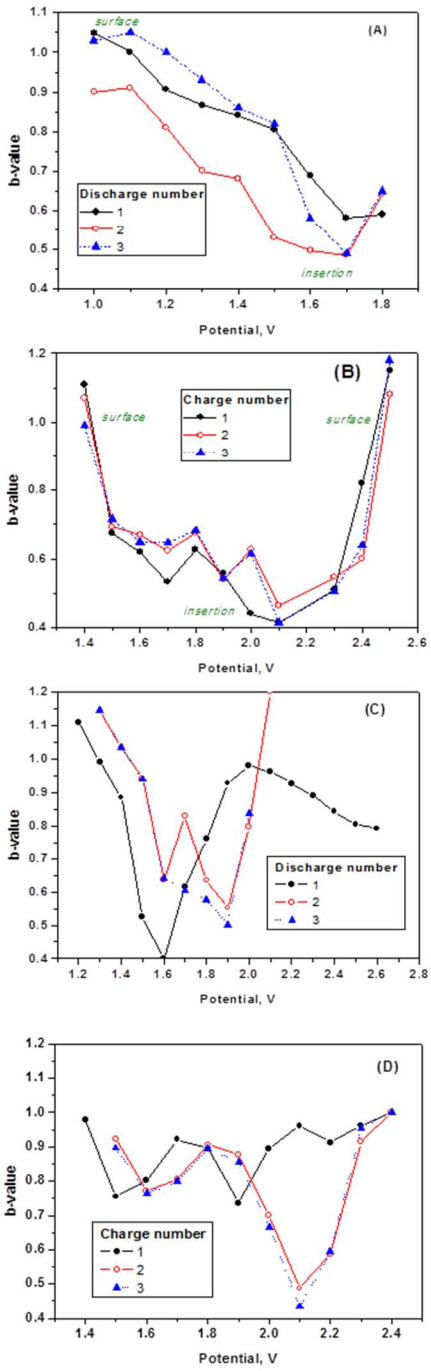

Fig. 7 Electrochemical b-values for SWANT a function of potential for discharge (A) and charge (B), and for DWANT during discharge (C) and charge (D) in lithium cell.

The b-parameter (Fig. 7) was extracted at several potential values and cycle number by analyzing cyclic voltammetry data. For the first three cycles of SWANT, the plot of b-parameter vs. potential shows a decreasing trend during discharge and approximately an U-shape on charge (Fig. 7A,B). In the 1.5-1.8 V region on discharge and 1.6-2.4 V on charge, the resulting b-values are close to 0.5, revealing diffusion-controlled faradaic processes due to Ti^{4+}/Ti^{3+} redox lithium insertion/extraction in anatase. In the 1.0-1.2 V region in discharge, and ca. 1.4 V and ca. 2.5 V on charge, b is close to 1.0, which indicates surface redox processes not controlled by lithium diffusion, including both faradaic pseudocapacitance and non-faradaic double layer effects. The differences between the electrochemical b-value in the discharge (Fig. 7A) and charge (Fig. 7B), are related to the hysteresis found on lithium insertion/extraction. These results are in good agreement with those found by Dunn's group for nanocrystalline film of anatase,[20] the main difference being a wider potential window where the insertion process takes place in SWANT. If we compare the results of SWANT (Fig. 7A,B) with those of DWANT (Fig. 7C, D), a significant increase in the values of the b-parameter is observed for DWANT, particularly during the charge process, and this fact would involve a higher contribution of the surface redox processes (pseudocapacitance not controlled by diffusion of lithium). These results are in very good agreement with the higher values of specific capacity found for DWANT (Fig. 4).

To summarize, the insertion of lithium into anatase takes place in the 1.5-1.8 V region, while the accommodation of lithium takes place in the surface of the nanotube in other voltage regions. Thus, the double-walled structure allows increasing the specific capacity in a wider potential range, as a result of the pseudocapacitive contributions in addition to the usual faradaic insertion process.

3.7 Electrochemical mechanism in sodium cell

The ability of anatase to react with sodium, which has been the subject of certain controversies, seems to be strongly affected by the morphology and size of the particles and, in fact, the mechanism is not well known.[12] Our previous studies about anatase nanotube in sodium cells revealed a very important contribution of the nanotube surface to the reversible capacity according to the obtained values of the b-parameter.[13] In addition, the ex-situ XRD pattern of the electrode DWANT after electrochemical cycling in sodium cell reveals that the anatase structure is preserved, in good agreement with the absence of extended plateaus in the potential-capacity curves, and in contrast with the biphasic transformation of anatase in lithium cell (see supplementary information). NMR, EPR and HRTEM can help to shed light on the study of the reaction between anatase nanotubes and sodium.

Irrespectively of the complex spectra that result from quadrupolar broadening, the observed ^{23}Na MAS NMR spectra of the SWANT and DWANT electrodes in the discharged state (Fig. 8) show a narrow peak placed at +5 ppm and broadened resonance centred at about – 11 ppm. These spectra are equivalent to others reported in the literature for sodiated TiO_2.[21,22] Thus, Suetake et al. ascribed a sharp peak at -2 ppm to sodium ions with high mobility and that interact weakly with the nt-TiO_2, while a broad signal at -10 ppm corresponds to sodium ions with restricted mobility and strongly associated with nt-TiO_2.[21] In Fig. 8, a certain narrowing of the signal for DWANT in comparison with SWANT is observed. A tentative explanation of this fact can be that the defects in SWANT (studied by EPR) can broaden the NMR signal. Another explanation is a better mobility of the sodium ions in the DWANT structure. Both possible interpretations are in good agreement with the higher values of specific capacity observed for DWANT in Fig. 4.

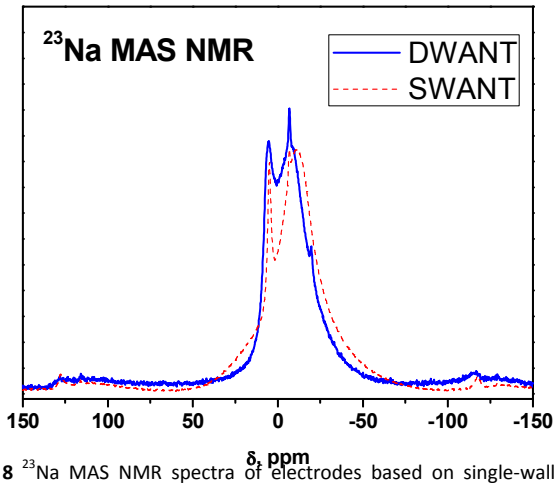

Fig. 8 ^{23}Na MAS NMR spectra of electrodes based on single-wall and double-wall anatase nanotubes discharged at 0.01 V vs. Na^+/Na.

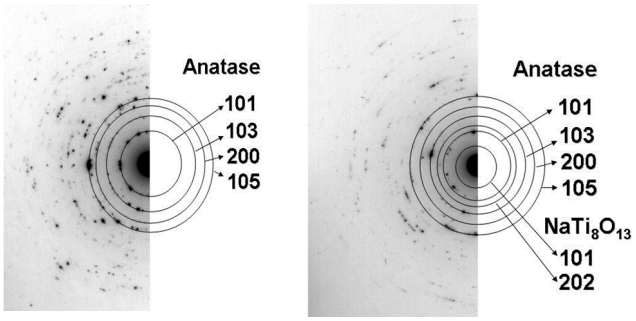

Fig. 9 Electron diffraction patterns for DWANT (left) and its sodiated counterpart (0 V vs. Na^+/Na, right).

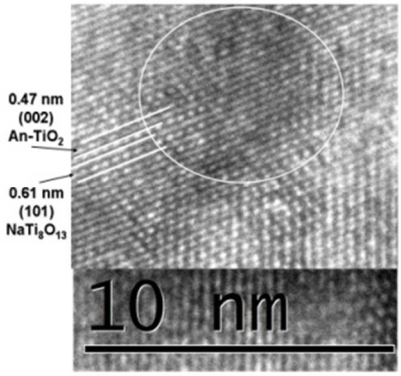

Fig. 10 HRTEM of sodiated DWANT. The anatase (An-TiO_2) and $NaTi_8O_{13}$ phases are indicated.

After the first discharge to 0.01 V in sodium cell, the recovered DWANT electrode was examined by TEM and electron diffraction patterns were recorded. Polycrystalline diffraction shows that sodiated DWANT consists of a mixture of anatase TiO_2 (main phase) and $NaTi_8O_{13}$ (minor component) (Fig. 9). Sodium titanate with $NaTi_8O_{13}$ stoichiometry is a Ti^{3+}/Ti^{4+} mixed valence compound that crystallizes in the R-3 space group.[23] It is worth to mention that the crystallinity of sodiated DWANT remains unchanged. Although it is not observed by ex-situ XRD of the recovered electrodes, the appearance of the crystalline impurity $NaTi_3O_8$ is evidenced by the HRTEM images: lattice fringes corresponding to (101) plane of $NaTi_8O_{13}$ are superimposed on the main lattice fringes due to (002) plane of the anatase TiO_2 (Fig. 10). The crystalline domain size of impurity $NaTi_8O_{13}$ spread up to 5 nm. However, this phase is observed with a relatively low frequency. The capacity associated with the formation of $NaTi_3O_8$ is too low to explain the higher specific capacity observed for DWANT in sodium cell. The distribution of all elements determined from high angle annular dark field TEM images are compared in Figure 11. It appears that Na, F and P are homogeneously distributed over the surface and inside the nanotubes. The atomic percentages of the elements are: Ti=32.5%, O=46.0%, Na=13.8%, F=5.6% and P= 2.1%. Thus, the EDS analysis shows that one sodium atom interacts with 2-3 Ti atoms from nt-TiO_2.

In comparison with the electrolyte solution of $NaPF_6$ salt in ED:DEC, the F/P ratio is lower than six. This gives an evidence for a partial decomposition of the electrolyte solution during the first discharge of DWANT.

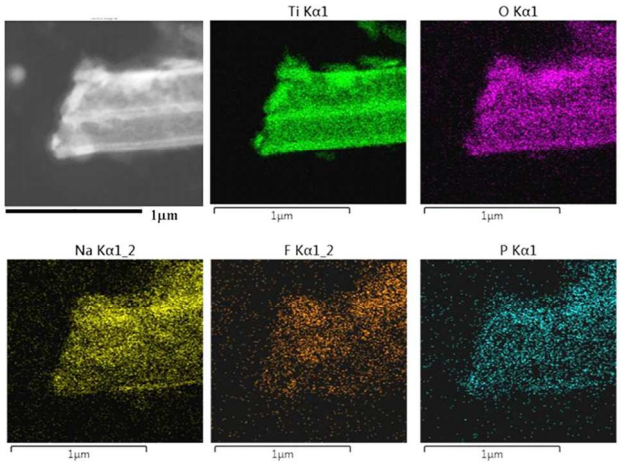

Fig. 11 High angle annular dark field TEM images and mapping of composition for Ti, O, Na, F and P.

The surface interaction between Na and nt-TiO_2 is further supported by the EPR results which are shown in Fig. 12. After sodiation of DWANT, the signal due to lattice electron trapping sites disappears and a new anisotropic signal with an average g=1.942 grows in intensity. The g-value is close to that observed for the signal due to surface anatase electron trapping sites. However, the appearance of the sodium titanate phase in the TEM results could be associated to the broad signal with Ti^{3+} in $NaTi_8O_{13}$. To check this assumption, we measure the EPR spectrum of sodiated DWANT after air exposition (Fig. 12). The EPR spectrum undergoes changes leading to the observation of two well resolved signals: a narrow asymmetric signal with $g_{\perp}$=1.985 and a broad symmetric signal with g=1.935. These two signals are characteristics of Ti^{3+} ions trapped in the regular lattice and surface sites of the anatase matrix, respectively. The observed changes in the EPR spectra imply that the broad signal of sodiated DWANT is due to Ti^{3+} in surface sites of the nanotubes, instead of $NaTi_8O_{13}$ which is thought to be stable under air.[20] On the other hand, Bandura et al. have recently demonstrated that nt-TiO_2 can integrate different crystalline phases in one and the same wall structure.[24]

In order to further highlight the role of the surface area to achieve high capacity, it is worth to remember that nt-TiO_2 also can be used like supercapacitor with aerial capacitance.[25]Thus, the pseudocapacitance due to absorption of lithium (and sodium) in the surface of the nanotube leads to an increase in the capacity of DWANT in comparison with a pure insertion process. Several authors have demonstrated the possibility of interfacial sodium (and lithium) storage in other materials.[26,27]

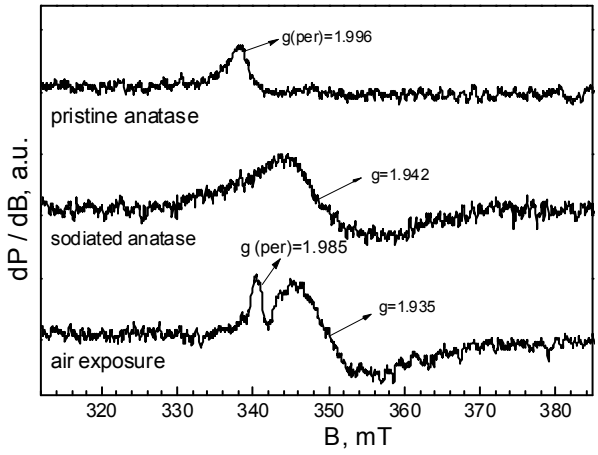

Fig. 12 EPR spectra for DWANT (20-100 V, 2 h) before and after its reaction with sodium. For the sake of comparison, the EPR spectrum of sodiated DWANT after exposing to air atmosphere for 1 day is also given.

4. Conclusions

Anodization under a voltage ramp is an easy method to prepare double-wall anatase nanotube using a single-step anodization process. The double-wall structure increases the specific capacity due to the pseudocapacitive contribution which is related to the higher surface coming from the special nanostructure, in addition to the usual faradaic insertion and in a wider potential range. The response to high current densities is improved with the double-wall structure. The initial smaller concentration of bulk defects (Ti^{3+} determined by EPR) in double-wall anatase is in good agreement with its higher specific capacity. The high specific capacity values make that this electrode materials can be

potentially very useful for lithium and sodium ion microbatteries. In the case of the reaction with sodium, the capacity of anatase is strongly related to the reduction to Ti^{3+} in the nanotube surface. Although the occurrence of Na_xTiO_2 phases is not detected by XRD, the presence of $NaTi_8O_{13}$ is inferred from TEM results. However, the main capacity of DWANT is associated with the nanotube surface interaction with Na instead of $NaTi_3O_8$ formation.

Acknowledgements

The authors are indebted to MEC (MAT2011-22753), Junta de Andalucía (FQM288). G.O. thanks MICINN for a Ramon y Cajal grant. E.Zh. and R.S. acknowledge the financial support from the National Centre for New Materials UNION (contract no. DCVP-02/2/2009).

Notes and references

[a] *Laboratorio de Química Inorgánica. Campus universitario de Rabanales, Edificio C3, Universidad de Córdoba. 14071 Córdoba, Spain. Fax: 34 957218621; Tel: 34 957218637, *E-mail: iq2alror@uco.es*

[b] *Institute of General and Inorganic Chemistry, Bulgarian Academy of Sciences, 113 Sofia, Bulgaria*

[c] *Institute of Mineralogy and Crystallography, Bulgarian Academy of Sciences,1113 Sofia, Bulgaria*

[d] *European Application Group, JEOL (Europe) SAS, 78290 Croissy-sur-Seine, France*

† Electronic Supplementary Information (ESI) available: [XRD and further electrochemical results]. See DOI: 10.1039/b000000x/

1 W. Wei, G. Oltean, C.W. Tai, K. Edström, F. Björefors and L. Nyholm, *J. Mater. Chem. A*, 2013, **1**, 8160.

2 J.R. González, R. Alcántara, F. Nacimiento, G.F. Ortiz, J.L. Tirado, E. Zhecheva and R. Stoyanova, *J. Phys. Chem. C*, 2012, **116**, 20182.

3 W.J.H. Borghols, D. Lützenkirchen-Hecht, U. Haake, E.R.H. van Eck, F.M. Mulder and M. Wagemaker, *PhysChemChemPhys.*, 2009, **11**, 5742.

4 S.Y. Huang, L. Kavan, I. Exnar and M. Grätzel, *J. Electrochem. Soc.*, 1995, **142**, L142.

5 N. Plylahan, M. Letiche, M.K.S. Barr, T. Djenizian, *Electrochem. Commun.*, 2014, **43**, 121.

6 V. Gentilli, S. Brutti, L.J. Hardwick, A.R. Armstrong, S. Panero and P.G. Bruce, *Chem. Mater.*, 2012, **24**, 4468.

7 M. Wagemaker, W.J.H. Borghols and F.M. Mulder, *J. Am. Chem. Soc.*, 2007, **129**, 4323.

8 G.F. Ortiz, I. Hanzu, P. Knauth, P. Lavela and J.L. Tirado, T. Djenizian, *Electrochim. Acta*, 2009, **54**, 4262.

9 S.K. Cheah, E. Perre, M. Rooth, M. Fondell, A. Harsta, L. Nyholm, M. Boman, T. Gustafsson, J.L.P. Simon and K. Edström, *Nano Lett.*, 2009, **9**, 3230.

10 S. P. Albu, H. Tsuchiya, S. Fujimoto and P. Smucki, *Eur. J. Inorg. Chem*., 2010, **27**, 4351.

11 J.R. González, R. Alcántara, G.F. Ortiz, F. Nacimiento and J.L. Tirado, *J. Electrochem. Soc.*, 2013, **160**, A1390.

12 L. Wu, D. Buchholz, D. Bresser, L. G. Chagas and S. Passerini, *J. Power Sources*, 2014, **251**, 379.

13 J.R. González, R. Alcántara, F. Nacimiento, G.F. Ortiz and J.L. Tirado, *CrystEngComm*, 2014, **16**, 4602.

14 D.C. Hurum, A.G. Agrios, K.A. Gray, T. Rajh and M.C. Thurnauer, *J. Phys. Chem. B*, 2003, **107**, 4545.

15 M. Fittipaldi, D. Gatteschi and P. Fornasiero, *Catal. Today*, 2013, **206**, 2.

16 D. C. Hurum, A.G. Agrios, S. E. Crist, K.A. Gray, T. Rajh and M.C. Thurnauer, *J. Electron. Spectrosc. Relat. Phenom.*, 2006, 150, 155.

17 N.A. Kyerematen, F. Dumur, P. Knauth, B. Pecquenard and T. Djenzian, *Electrochem. Commun.*, 2011, **13**, 894.

18 J.Y. Shin, D. Samuelis and J. Maier, *Solid State Ionics,* 2012, **225**, 590.

19 J. Wang, J. Polleux, J. Lim and B. Dunn, *J. Phys. Chem. C*, 2007, **111**, 14925.

20 T. Brezesinski, J. Wang, J. Polleux, B. Dunn and S.H.J. Tolbert, *J. Am. Chem. Soc.*, 2009, **131**, 1802.

21 J. Suetake, A.Y. Nosaka, K. Hodouchi, H. Matsubara and Y. Nosaka, *J. Phys. Chem. C*, 2008, **112**, 18474.

22 A.Y.H. Lo, R.W. Schurko, M. Vettraino, B.O. Skadtchenko, M. Trudeau and D.M. Antonelli, *Inorg. Chem.*, 2006, 45, 1828.

23 J. Akimoto and H. Takei, *J. Solid State Chem.*, 1991, **90**, 147.

24 A.V. Bandura, R.A. Evarestov and S.I. Lukyanov, *ChemPhysChem*, 2014, **16**, 14781.

25 M. Salari, S.H. Aboutalebi, A.T. Chidembo, I.P. Nevirkovets, K. Konstantinov and H.K. Liu, *PhysChemChemPhys*, 2012, **14**, 4770.

26 W.M. Liu, Q. Sun and Z.W. Fu,, Electrochem. Commun, 2013, **27**, 156.

27 J. Jamnik and J. Maier, *PhysChemChemPhys*, 2003, **5**, 5215.